Available online at www.sciencedirect.com
SCIENCE DIRECT®
International Journal of Heat and Fluid Flow 25 (2004) 749–758
International Journal of HEAT AND FLUID FLOW
www.elsevier.com/locate/ijhff

Direct numerical simulation of turbulent heat transfer in plane impinging jet

Hirofumi Hattori *, Yasutaka Nagano

Department of Mechanical Engineering, Nagoya Institute of Technology, Gokiso-cho, Showa-ku, Nagoya 466-8555, Japan

Received 23 January 2004; accepted 21 May 2004
Available online 25 August 2004

Abstract

The objectives of this study are to investigate the structures and characteristics of flows and heat transfer for plane turbulent impinging jets in a confined space, where a wall-jet type of flow is influenced by both lower (impingement) and upper walls, and to obtain turbulent statistics for the construction of a turbulent heat transfer model. For these purposes, we have performed direct numerical simulations (DNS) of impinging flows with heat transfer. To obtain the effects of an impingement distance on heat transfer, the value of H is changed in calculations, where H is the distance between the impingement wall and the upper wall. It is found from the present DNS that the Nusselt number increases with a decrease in the distance H similar to the experimental results. In addition, the Nusselt number of the case with the highest distance decreases monotonously in the wall-jet development direction, while in shorter distance cases the second peak of the Nusselt number is clearly observed away from the stagnation point, due to the increase in wall-normal turbulence intensities in the region away from the stagnation point.

Keywords: Impingement; Plane jet; Turbulence; Heat transfer; Direct numerical simulation

1. Introduction

It is well known that the characteristics of local heat transfer are improved in the round impingement jet with low nozzle-plate spacing (see Viskanta, 1993; Lytle and Webb, 1994). Though impingement jets have been studied in detail by many researchers (e.g., Cooper et al., 1993; Ichimiya et al., 1987; Nishino et al., 1996; Sakakibara et al., 1997; Satake and Kunugi, 1998; Sakakibara et al., 2001; Tsubokura et al., 2003), almost all of their studies concern a round impingement jet. Therefore, it is not clear whether local heat transfer is improved by low nozzle-plate spacing in a plane impingement jet. On the other hand, an impinging jet in a confined space is an important phenomenon for problems relevant to engineering. In order to obtain a more detailed knowledge of both the velocity and thermal fields in plane turbulent impingement jets with low nozzle-plate spacing and statistical turbulence quantities in fields for the construction of turbulent heat transfer model, we conducted direct numerical simulations (DNS) of these flows with heat transfer under various nozzle-plate spacing conditions. The structures, characteristics and transport mechanisms of flows and heat transfer in the velocity and thermal fields are investigated using the DNS. In particular, the second peak of local heat transfer coefficient (Nusselt number) appears in the case of very low nozzle-plate spacing (Cooper et al., 1993; Ichimiya et al., 1987; Lytle and Webb, 1994). The mechanism for the origin of this phenomenon is also discussed in detail.

2. Numerical procedure

Fig. 1 shows a schematic plane impinging jet and the coordinate system used in the present study. DNS based on the finite-difference method was carried out under conditions of $Re_m = 9120$ and $Pr = 0.71$.

The velocity field is governed by the incompressible Navier–Stokes equation without buoyancy and the continuity equation, which are non-dimensionalized by

* Corresponding author. Tel./fax: +81-52-735-5359.
E-mail address: hattori@heat.mech.nitech.ac.jp (H. Hattori).

0142-727X/$ - see front matter © 2004 Elsevier Inc. All rights reserved.
doi:10.1016/j.ijheatfluidflow.2004.05.004

Nomenclature

C_f	local skin friction coefficient, $2\tau_w/(\rho V_m^2)$
c_p	specific heat at constant pressure
D	inlet channel width
h	local heat transfer coefficient, $q_w/\Delta\Theta$
H	impingement distance
H_L	length of wall-jet development direction
H_Z	spanwise length
k	turbulence energy, $\overline{u_i u_i}/2$
n_i	grid numbers in x_i direction
Nu	Nusselt number, $2hD/\lambda$
p	pressure
Pr	Prandtl number, ν/α
q_w	wall heat flux, $-\lambda(\partial\overline{\Theta}/\partial y)\big\|_w$
Re_m	Reynolds number based on mean velocity and hydraulic diameter of inlet channel, $2V_m D/\nu$
t	time
$\overline{U}_i$	mean velocity in x_i direction
u_i	instantaneous velocity or velocity fluctuation in x_i direction
$\overline{U}$	mean velocity in streamwise direction
u, v, w	velocity fluctuation in streamwise, impingement wall-normal and spanwise directions, respectively
V_m	mean velocity at inlet channel
x, y, z	coordinate in streamwise, impingement wall-normal and spanwise directions
u_τ	friction velocity, $\sqrt{\tau_w/\rho}$

Greek symbols

α	thermal diffusivity, $\lambda/(\rho c_p)$
$\Delta\theta$	reference temperature, $q_w/(\rho c_p V_m)$
$\Delta\Theta$	temperature difference between inlet and impingement wall, $\Theta_{wall} - \Theta_0$
$\overline{\Theta}$	mean temperature
θ	instantaneous temperature or temperature fluctuation
θ_{rms}	temperature variance, $\sqrt{\overline{\theta^2}}$
θ_τ	friction temperature, $q_w/(\rho c_p u_\tau)$
Θ_{wall}	mean temperature at impingement wall
Θ_0	mean temperature at inlet channel
λ	thermal conductivity
μ	coefficient of viscosity
ν	coefficient of kinematic viscosity
ρ	density
τ_w	wall shear stress, $\mu(\partial\overline{U}/\partial y)\big\|_w$

Subscripts and superscripts

$\overline{(\ )}$	ensemble and time-averaged value
$(\ )^*$	normalization by inlet mean velocity, V_m, inlet channel width, D, and reference temperature, $\Delta\theta$
$(\ )^+$	normalization by local inner variables, u_τ, θ_τ and ν

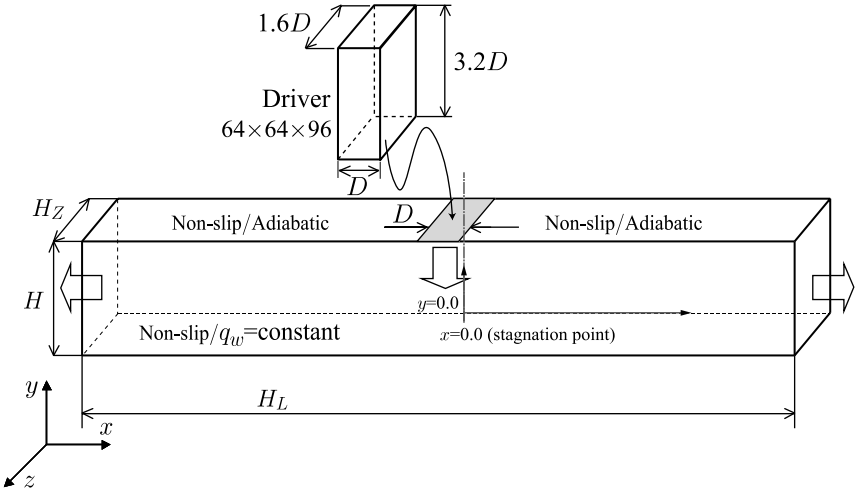

Fig. 1. Flow and thermal conditions and coordinate system.

the mean velocity V_m at the nozzle and the channel width D. They are given as follows:

$$\frac{\partial u_i^*}{\partial x_i^*} = 0 \tag{1}$$

$$\frac{\partial u_i^*}{\partial t^*} + u_j^* \frac{\partial u_i^*}{\partial x_j^*} = -\frac{\partial p^*}{\partial x_i^*} + \frac{2}{Re_m}\frac{\partial^2 u_i^*}{\partial x_j^* \partial x_j^*} \tag{2}$$

Table 1
Grid points and computational domain

	Grid points ($x \times y \times z$)	Computational domain ($H_L \times H \times H_Z$)
Case 1	340×96 ×96	$26D \times 2D \times 1.6D$
Case 2	320×96 ×96	$21D \times 1D \times 1.6D$
Case 3	320×96 ×96	$21D \times 0.5D \times 1.6D$

Table 2
Grid spaces in wall units

	Case 1	Case 2	Case 3
Δx^+	1.49–48.9	1.88–51.5	2.76–86.5
Δy^+	0.20–26.9	0.09–15.8	0.05–11.4
Δz^+	1.66–9.17	1.48–10.8	1.53–15.6

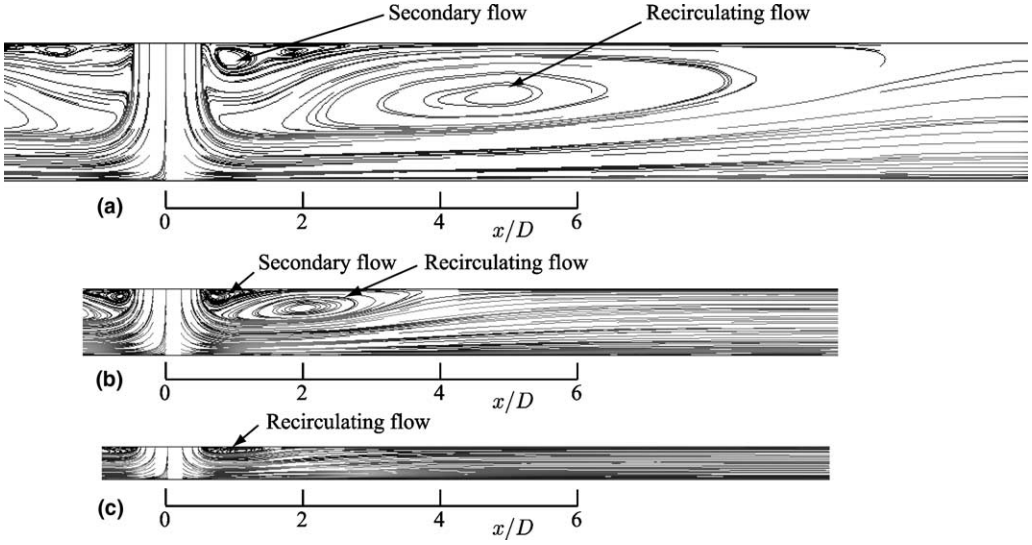

Fig. 2. Flow trajectories: (a) Case 1, (b) Case 2 and (c) Case 3.

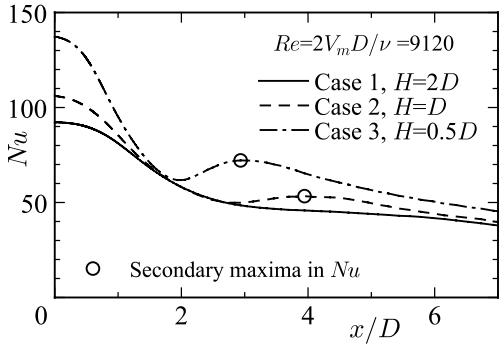

Fig. 3. Distributions of local Nusselt number in plane impinging jet.

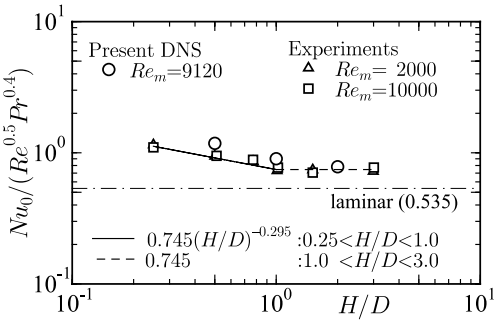

Fig. 4. Dependence of Nusselt number at stagnation point on nozzle-plate spacing ratio.

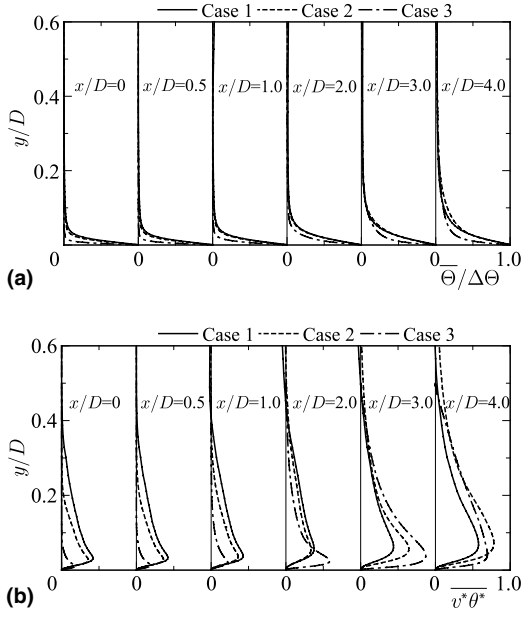

Fig. 5. Profiles of mean temperature and wall-normal turbulent heat-flux: (a) mean temperatures and (b) turbulent heat-fluxes.

The energy equation governing the thermal field non-dimensionalized with the temperature difference $\Delta\theta = q_w/(\rho c_p V_m)$ is as follows:

$$\frac{\partial\theta^*}{\partial t^*} + u_j^* \frac{\partial\theta^*}{\partial x_j^*} = \frac{2}{PrRe_m} \frac{\partial^2\theta^*}{\partial x_j^* \partial x_j^*} \tag{3}$$

The inlet flow condition is given by the fully developed turbulent channel flow DNS simulation so as to exclude the inlet anomalous effect. The boundary conditions include the following: non-slip conditions for the velocity field at walls, constant heat-flux conditions at the impingement surface, an adiabatic wall condition on the other wall for the thermal field, periodic conditions in spanwise directions; the time-dependent condition of any velocity component, u_i, and temperature, θ, at the exit plane, which is given as $\partial\phi/\partial t + U_c\partial\phi/\partial x = 0$, where U_c is the constant bulk exit velocity (convection velocity), and $\phi = u_i, \theta$ (Le et al., 1997). Three cases of nozzle-plate spacing, H, and computational domain are arranged as shown in Table 1, in which the nozzle-plate spacing, $H = 2D$, and the length of the flow developing region, $H_L = 26D$ in Case 1, $H = 1D$ and $H_L = 21D$ in Case 2, and $H = 0.5D$ and $H_L = 21D$ in Case 3, are given. The grid points are arranged as shown in Table 1 for individual case. In the discretization of equations, the 2nd-order central finite-difference is used for space, and the 2nd-order Adams–Bashforth method is used for time (Nagano et al., 2004). In order to couple the continuity equation with the momentum equation, the fractional-step method is used. The numerical scheme used in this study is validated by comparing the statistical quantities in plane channel flow with those calculated in our group's DNS (Nagano and Hattori, 2003), which employs the spectral method.

3. Results and discussion

3.1. Fundamental turbulent statistics

In the calculation of an impinging jet, the wall units vary along the wall-jet development direction. There-

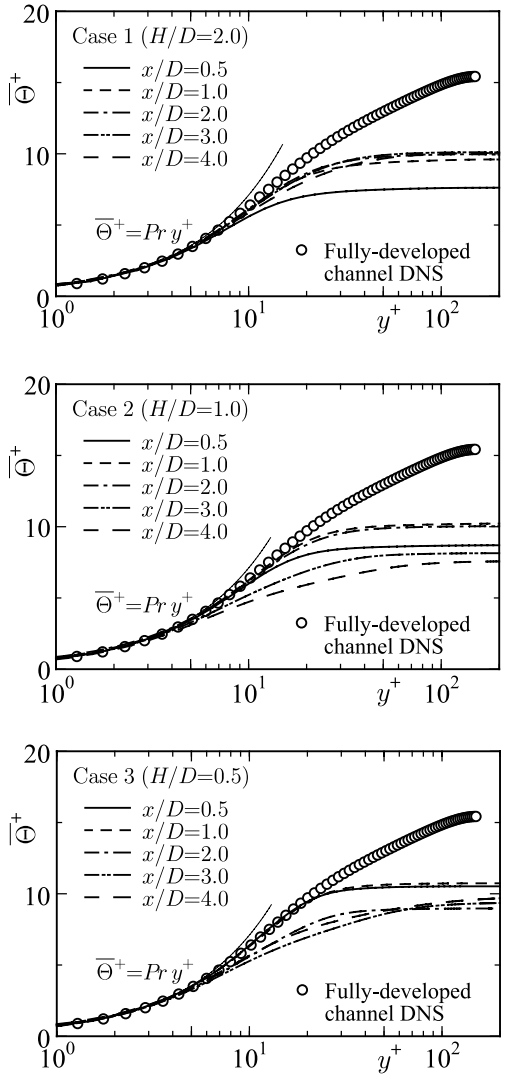

Fig. 6. Distributions of mean temperature in wall unit.

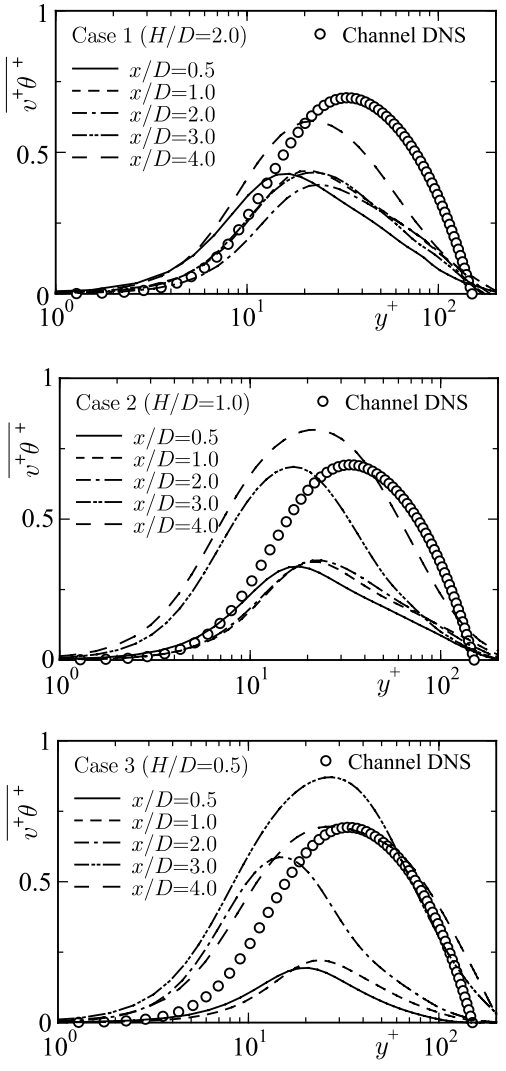

Fig. 7. Distributions of wall-normal turbulent heat-flux in wall unit.

fore, special attention was paid to the grid spacing to enable a more accurate DNS appraisal. According to the present DNS, grid spaces by the wall unit are shown in Table 2. Note that since a non-uniform grid is employed for the x and y directions, the grid spacing becomes large toward the exit plane and center of the channel. Therefore, the grid spacing used in our DNS should be adequate to capture the phenomena of target heat transfer, i.e., an occurrence of the second peak of local heat transfer coefficient.

Fig. 2 shows the flow trajectories of mean velocity. The flow field for each case is formed into a main flow and a recirculating flow yielded by the main flow and a secondary flow between the impinging jet and the recirculating flows. The secondary flow is caused by the existence of the upper wall. However, the secondary flow is not found in Case 3 clearly as shown in Fig. 2(c). The wall-jet flow of Case 3 is observed to develop fastest among all cases. These phenomena affect the turbulence statistics discussed below.

The distributions of local Nusselt number defined as $Nu = 2hD/\lambda$ are shown in Fig. 3. Also, Fig. 4 shows the dependence of Nusselt numbers at stagnation point on nozzle-plate spacing ratio as compared with experimental data (Ichimiya et al., 1987). It is found that the present DNS captures the local Nusselt number at the stagnation point in the case of low nozzle-plate spacing measured experimentally (Ichimiya et al., 1987). Moreover, the local Nusselt number in Case 3 is largest in all cases at the stagnation point indicated in Fig. 1. In addition, though the local Nusselt number in Case 1 decreases monotonously in the wall jet developing direction, the second peaks of the local Nusselt number are observed to be away from the stagnation point in

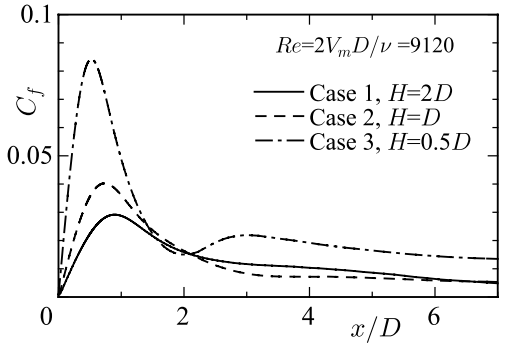

Fig. 8. Distributions of local skin friction coefficient in plane impinging jet.

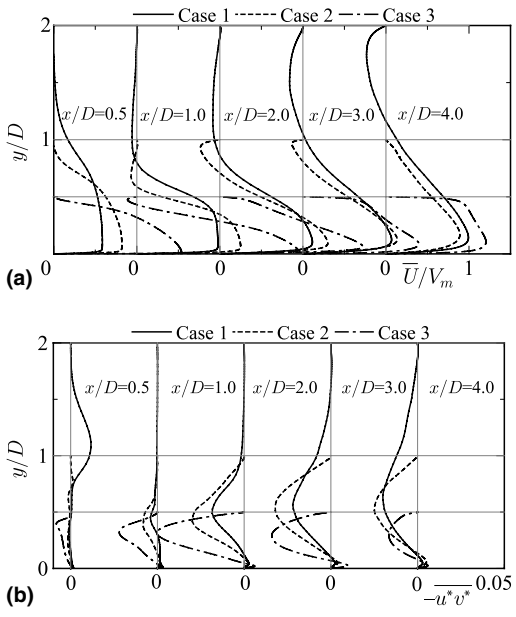

Fig. 9. Profiles of streamwise mean velocity and Reynolds shear stress: (a) mean velocities and (b) Reynolds shear stresses.

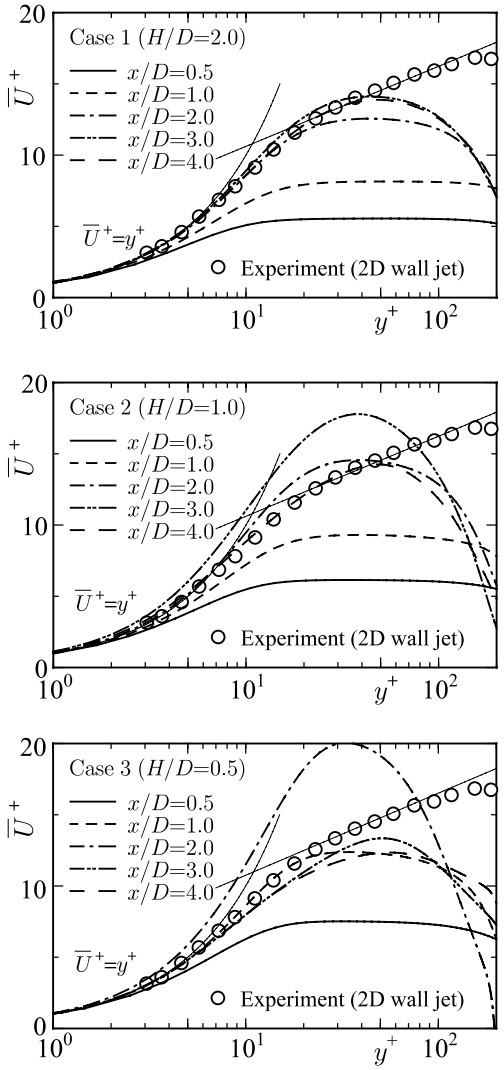

Fig. 10. Distributions of streamwise mean velocity in wall unit.

Cases 2 and 3 similar to the experimental data (Lytle and Webb, 1994; Cooper et al., 1993).

The distributions of turbulence quantities for thermal field in the wall jet developing region are shown in Figs. 5–7. The profiles of mean temperature, $\Theta/\Delta\Theta$, and the wall-normal turbulent heat-flux, $\overline{v^*\theta^*}$, are indicated in Fig. 5(a) and (b), respectively. Also, profiles of mean temperature, Θ/t_τ, and wall-normal turbulent heat-flux, $\overline{v\theta}/(u_\tau t_\tau)$, are shown in Figs. 6 and 7. At the stagnation point ($x/D = 0$), the high heat transfer rates are accomplished by coherent vortical structures near the lower wall transporting the heat from the lower wall (e.g., Sakakibara et al., 1997). In the present DNS, the wall-normal turbulent heat-flux develops quickly in Cases 2 and 3 in the wall jet developing region. In particular, at the near point where the second peak of the local Nusselt number occurs, the wall-normal turbulent heat-flux affects apparently the second peak of the local Nusselt number in Cases 2 and 3. The occurrence of the second peak of the local Nusselt number is discussed in detail in the following section.

For the velocity field, the local skin friction coefficient defined as $C_f = \tau_w/(\rho V_m^2/2)$ is shown in Fig. 8. The largest local skin friction coefficient appears in Case 3 around the stagnation point ($x/D < 2$). After this point, the local skin friction coefficient of Case 3 decreases rapidly, becoming the largest in all cases in the wall jet developing region ($x/D > 2$). In particular, the second peak of the local skin friction coefficient is only observed in Case 3. Fig. 9 shows the distributions of the streamwise mean velocity and the Reynolds shear stress. The negative value of Reynolds shear stress corresponded to streamwise mean velocity profiles developed in the upper wall or recirculation region. On the other hand, the streamwise mean velocity profiles normalized by local friction velocity are shown in Fig. 10 with experimental data on 2D wall jet (Karlsson et al., 1993) for comparison. It can be seen that mean the velocities of Case 1 agree with experimental data of 2D wall jet in the region $x/D > 2.0$, but those of Cases 2 and 3 are not in agreement with the

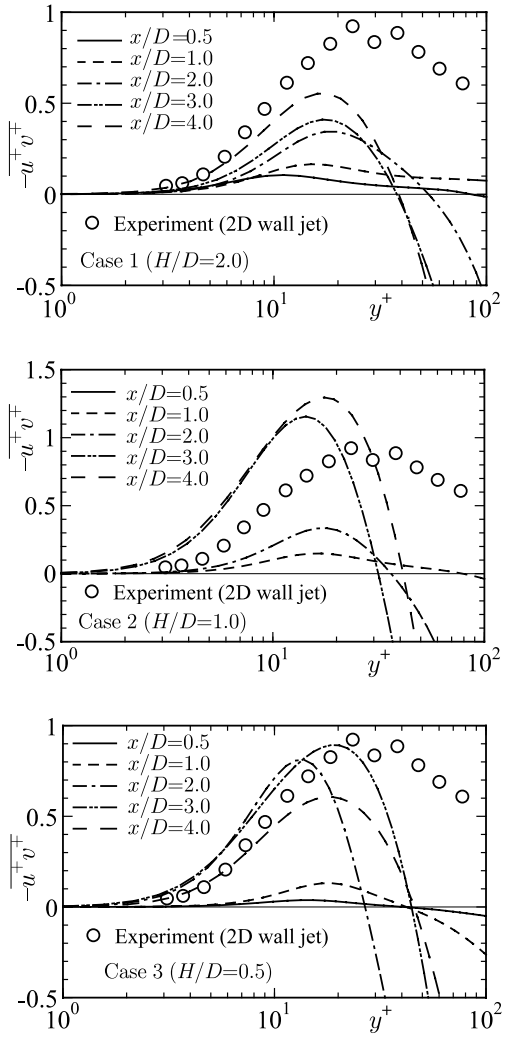

Fig. 11. Distributions of Reynolds shear stress in wall unit.

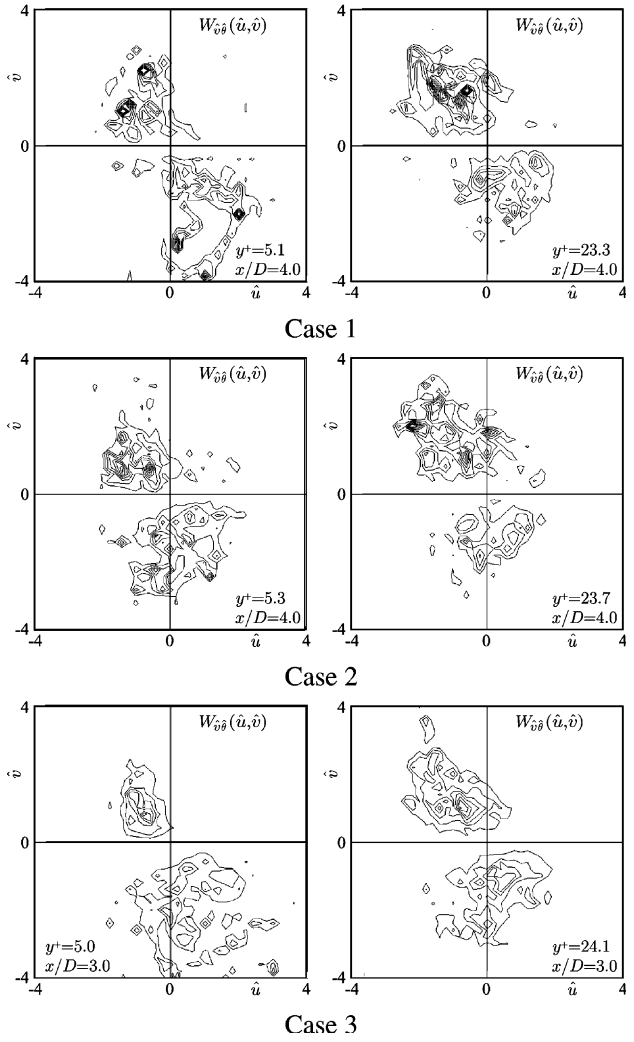

Fig. 12. Weighted p.d.f of $\overline{v\theta}$.

experimental data of 2D wall jet. In particular, the clear-cut log region is not observed in Cases 2 and 3. Near-wall distributions of Reynolds shear stress in wall unit are indicated in Fig. 11. Also, the experimental data of 2D wall jet are included. It can be observed that the Reynolds shear stresses of Cases 2 and 3 develop remarkably in the near-wall region. Obviously, the peculiar distributions of local skin friction coefficient correspond with these distributions.

4. Second peak of heat transfer rate and turbulence structure

This section discusses the peculiar distribution of the heat transfer rate (local Nusselt number) in Cases 2 and 3, namely the occurrence of a second peak, and its related turbulence structures. First, the reason for the enhancement of the wall-normal turbulent heat-flux is investigated. In order to associate each fluid motion in

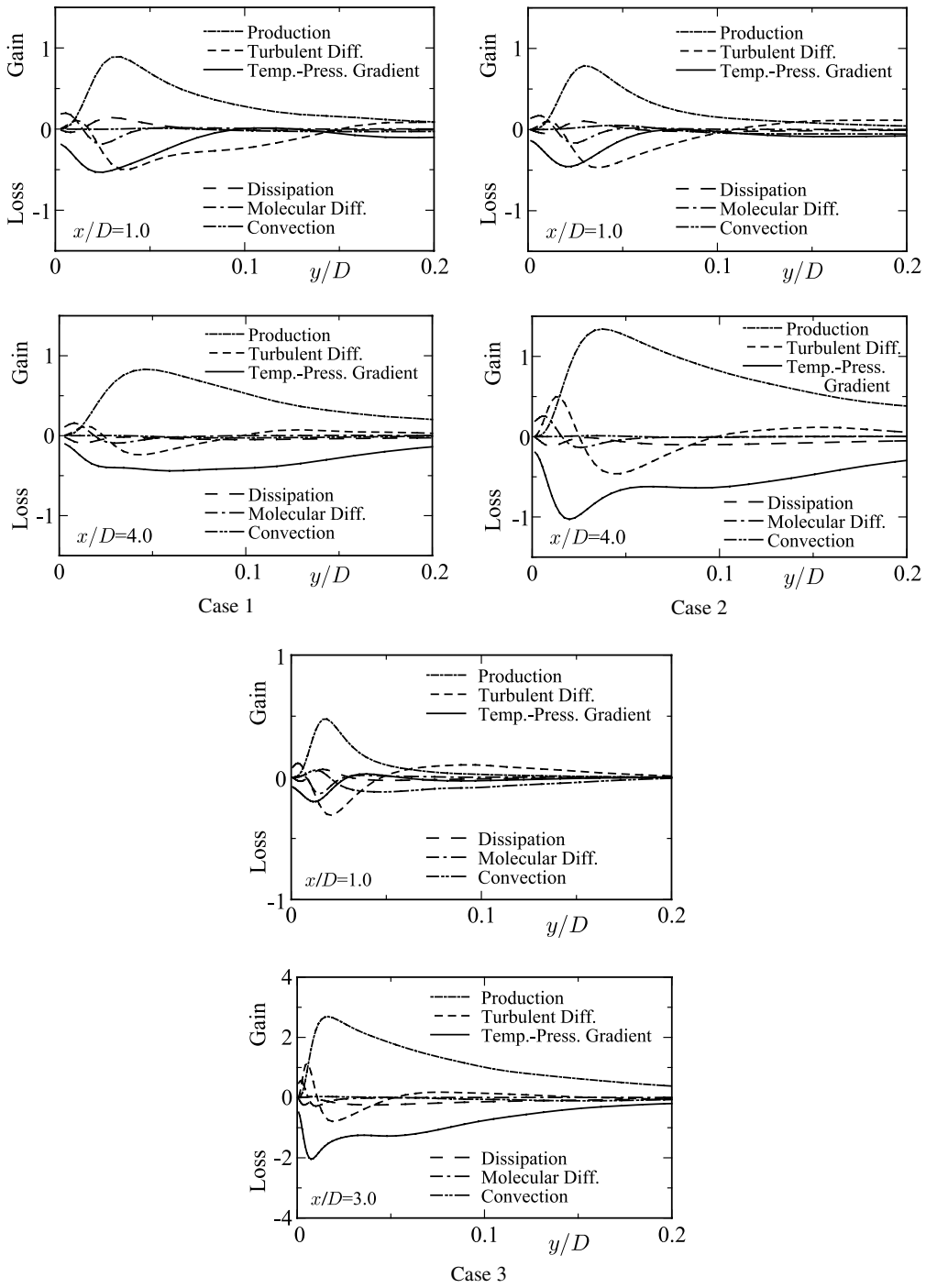

Fig. 13. Budgets of transport equation for wall-normal turbulent heat-flux.

the quadrants of the (u, v)-plane with the wall-normal turbulent heat-flux, the weighted p.d.f. of $\overline{v\theta}$ in the (u, v)-plane near the second peak point is defined by the following equation (Nagano and Tagawa, 1988) and shown in Fig. 12.

$$W_x(\hat{u}, \hat{v}) = \int_{-\infty}^{\infty} xP(\hat{u}, \hat{v}, \hat{\theta})\,\mathrm{d}\hat{\theta} \tag{4}$$

$x = \hat{v}\hat{\theta}$

It is obvious that the wallward interaction motion relating to sweeps contributes mainly to the wall-normal heat flux in the vicinity of the wall ($y^+ \simeq 5.0$) in Cases 2 and 3. In the log region ($y^+ \simeq 24$), the ejection motion becomes active in all cases. However, the wallward interaction motion still contributes to the wall-normal heat flux in Case 3.

Fig. 13 shows the budgets of the transport equation for the wall-normal turbulent heat-flux at $x/D = 1.0$, where the local Nusselt numbers of Cases 2 and 3 decrease and almost agree with that of Case 1, and at $x/D = 3.0$ or 4.0, where the second peak of the local Nusselt number appears. Also, in Fig. 13, the production and turbulent diffusion terms of Cases 2 and 3 more greatly affect the activation of the wall-normal turbulent heat-flux near the wall as compared with Case 1, although the contributions of these terms are similar at $x/D = 1.0$. The production term, $P_{v\theta}$, and turbulent diffusion term, $T_{v\theta}$, of the wall-normal turbulent heat-flux are given by the following equations:

$$P_{v\theta} = -\overline{v}^2 \frac{\partial \overline{\Theta}}{\partial y} - \overline{v\theta}\frac{\partial \overline{V}}{\partial y} \tag{5}$$

$$T_{v\theta} = \frac{\partial \overline{v^2\theta}}{\partial y} \tag{6}$$

Obviously, according to Eqs. (5) and (6), the effective turbulence quantity for these terms is the wall-normal turbulence intensity, $\overline{v}^2$. This is also concluded from the results of the weighted p.d.f. shown as Fig. 12. Fig. 14 shows the distributions of the wall-normal turbulence intensity near the wall in the x direction. The enhancement of the wall-normal turbulence intensities of Cases 2 and 3 clearly appear in the region near the second peak points close to the wall. Similarly, in comparison with Case 1, the turbulence intensities of Cases 2 and 3 are obviously promoted at $x/D = 3.0$ and 4.0 as shown in Fig. 15.

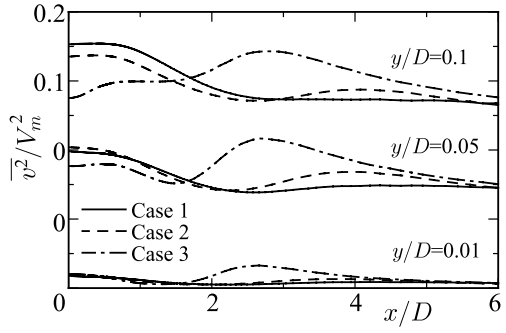

Fig. 14. Near-wall distributions of wall-normal turbulence intensities in x direction.

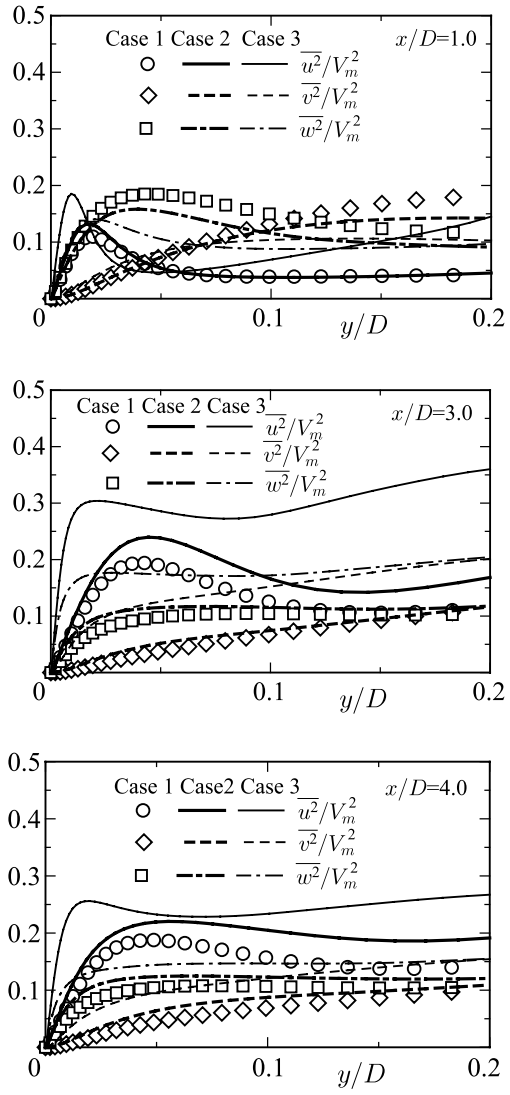

Fig. 15. Distributions of turbulence intensities.

Moreover, in order to investigate the enhancement of turbulence intensities for Cases 2 and 3, the budgets of the transport equation for turbulence intensities at $x/D = 3.0$ or 4.0 are shown in Figs. 16–18. Although the streamwise turbulence intensity $\overline{u}^2$ redistributes the turbulence energy to the wall-normal and the spanwise turbulence intensities through the pressure strain term normally, the wall-normal turbulence intensity also is found to distribute the spanwise turbulence intensity near the wall similar to the near-wall phenomena of turbulent plane channel flow (Iida and Nagano, 1998). The budget of the wall-normal turbulence intensities for Cases 2 and 3 are dominated mainly by the pressure

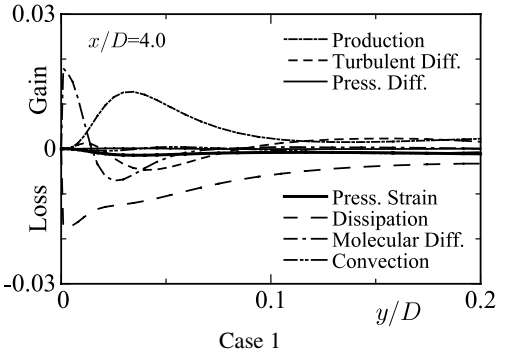

Case 1

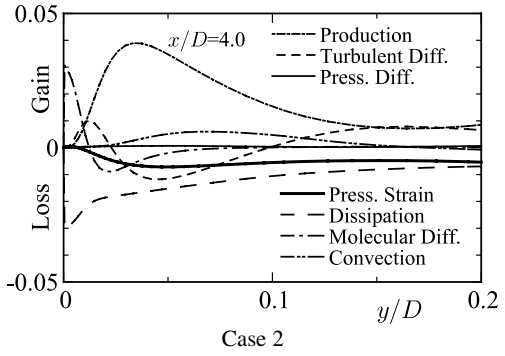

Case 2

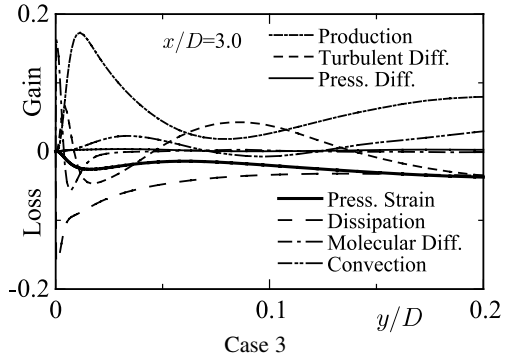

Case 3

Fig. 16. Budgets of transport equation for turbulence intensities, $\overline{u}^2$.

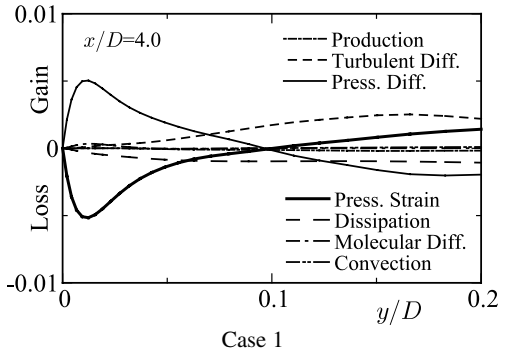

Case 1

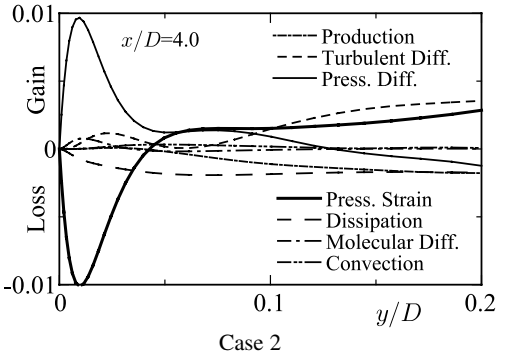

Case 2

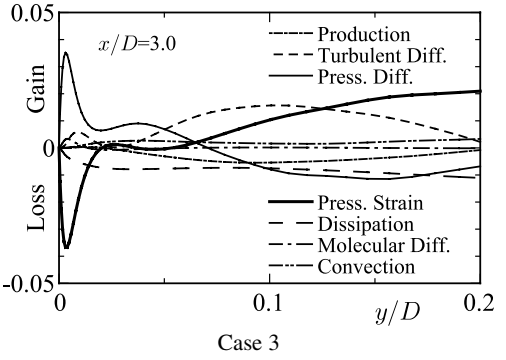

Case 3

Fig. 17. Budgets of transport equation for turbulence intensities, $\overline{v}^2$.

diffusion and the pressure strain (redistribution) terms in the vicinity of the wall. In comparison with Case 1, the pressure and turbulent diffusion terms are active near the wall as indicated in Fig. 17. Thus, strong wall-normal turbulence intensities appear when viewing the region.

Based on the foregoing, it is concluded that the turbulent diffusions of both the wall-normal heat-flux and turbulence intensity, the production of the wall-normal heat-flux, and the pressure diffusion of the wall-normal turbulence intensity, all play a key role in the occurrence of the second peak of the local heat transfer rate (Nusselt number).

5. Conclusions

We observed the effects of nozzle-plate spacing in plane impingement jets using the DNS. It was found that the second peak of the local heat transfer rate (Nusselt number) in the wall jet developing region appears in the lower nozzle-plate spacing case as observed in the experiment, which cannot be observed with wide spacing. Also, it is observed that the skin friction coefficient in the case of the lowest nozzle-plate spacing has a second peak similar to the heat transfer rate. Moreover, the turbulent transport phenomena and mechanism of the plane impingement jet are discussed in detail. In particular, the mechanism for the occurrence of the second peak of the local Nusselt number is mentioned, in which the phenomenon is influenced by the development of the wall-normal heat-flux near the wall. Therefore, to investigate this phenomenon, the budget of the wall-normal heat-flux is shown, in which it can be seen that the production and turbulent diffusion terms serve to enhance the wall-normal heat-flux. Since

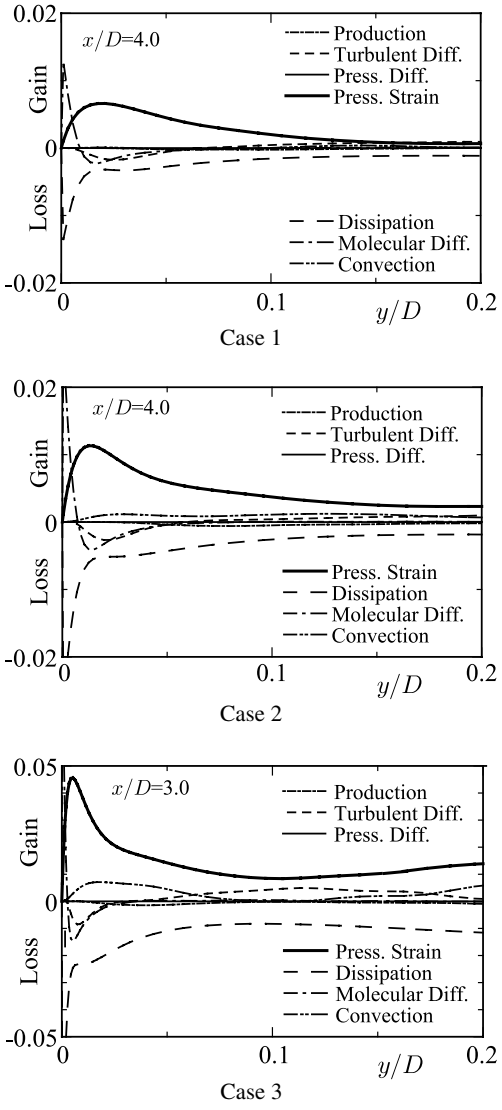

Fig. 18. Budgets of transport equation for turbulence intensities, $\overline{w}^2$.

these terms include the wall-normal turbulence intensity, we also explore turbulence intensities. It is found that the wall-normal turbulence intensity is promoted close to the wall near the region, where the second peak of the local Nusselt number occurs.

The present DNS provide detailed information on turbulence quantities including the budgets of their transport equations. Therefore, these DNS will be useful for the construction of a turbulence model, which will be the subject of a forthcoming paper.

Acknowledgement

The authors gratefully acknowledge the support provided for part of this research by Japan Atomic Energy Research Institute (JAERI).

References

Cooper, D., Jackson, D.C., Launder, B.E., Liao, G.X., 1993. Impinging jet studies for turbulence model assessment—I. Flow-field experiments. Int. J. Heat Mass Transfer 36, 2675–2684.

Ichimiya, K., Kobayashi, K., Echigo, R., 1987. Fundamental study on the flattening of temperature distribution of a high temperature steel slab (3rd report, heat transfer characteristics due to a confined turbulent impinging jet flow). Trans. JSME 53, 511–515 (in Japanese).

Iida, O., Nagano, Y., 1998. The relaminarization mechanisms of turbulent channel flow at low Reynolds numbers. Flow Turbul. Combust. 60, 193–213.

Karlsson, R.I., Eriksson, J., Persson, J., 1993. An experimental study of a two dimensional plane turbulent wall jet. Vattenfall Utveckling AB.

Le, H., Moin, P., Kim, J., 1997. Direst numerical simulation of turbulent flow over a backward-facing step. J. Fluid Mech. 330, 349–374.

Lytle, D., Webb, B.W., 1994. Air jet impingement heat transfer at flow nozzle-plate spacing. Int. J. Heat Mass Transfer 37, 1687–1697.

Nagano, Y., Hattori, H., 2003. DNS and modelling of spanwise rotating channel flow with heat transfer. J. Turbul. 4 (010), 1–15.

Nagano, Y., Tagawa, M., 1988. Statistical characteristics of wall turbulence with a passive scalar. Int. J. Fluid Mech. 196, 157–185.

Nagano, Y., Hattori, H., Houra, T., 2004. DNS of velocity and thermal fields in turbulent channel flow with transverse-rib roughness. Int. J. Heat Fluid Flow 25, 393–403.

Nishino, K., Samada, M., Kasuya, K., Torii, K., 1996. Turbulence statistics in the stagnation region of an axisymmetric impinging jet flow. Int. J. Heat Fluid Flow 17, 193–201.

Sakakibara, J., Hishida, K., Maeda, M., 1997. Vortex structure and heat transfer in the stagnation region of an impinging plane jet (simultaneous measurements of velocity and temperature fields by digital particle image velocimetry and laser-induced fluorescence). Int. J. Heat Mass Transfer 40 (13), 3163–3176.

Sakakibara, J., Hishida, K., Phillips, W.R.C., 2001. On the vortical structure in a plane impinging jet. J. Fluid Mech. 434, 273–300.

Satake, S., Kunugi, T., 1998. Direct numerical simulation of an impinging jet into parallel disks. Int. J. Numer. Methods Heat Fluid Flow 8, 768–780.

Tsubokura, M., Kobayashi, T., Taniguchi, N., Jones, W.P., 2003. A numerical study on the eddy structures of impinging jets excited at the inlet. Int. J. Heat Fluid Flow 24, 500–511.

Viskanta, R., 1993. Heat transfer to impinging isothermal gas and flame jets. Exp. Thermal Fluid Sci. 6, 111–134.